Simulated Feasibility of 3-D Lightning Mapping From Space

Jackson R. Remington, *Member, IEEE*, Patrick N. Gatlin, *Member, IEEE*, Sarah M. Stough, Nikhil Pailoor, Sonja A. Behnke, Timothy J. Lang, and Harald E. Edens

***Abstract*— In addition to the awe it inspires, lightning can illuminate the microphysical processes hidden away within deep convection. The current generation of space-based lightning mapping uses mostly 2-D optical imaging to connect overall flash characteristics to their parent storm dynamics, but are missing a dimension's worth of information. With lightning now classified as an essential climate variable, future spaceborne mappers will need improved capabilities to take advantage of the 3-D structure of lightning flashes to support meteorological and climate modeling. We report here on a study of the feasibility of high-resolution 3-D lightning mapping using a radio frequency (RF)-based network of satellites from low-Earth orbit (LEO). Lightning sources are simulated using existing lightning mapping array (LMA) tools, modified for orbital detection, and spatially reconstructed using a Levenberg–Marquardt geolocation algorithm to assess sources of uncertainty in these solutions. We analyze the benefits and limitations of this approach compared to existing orbital and ground-based methods. Results of this study show that lightning can be mapped in 3-D with a vertical location accuracy better than 2 km using as few as five satellites in LEO capable of measuring the time-of-arrival of impulsive RF signals in the very high-frequency (VHF) band. The consequence of this study is that high-resolution, spaceborne 3-D mapping of lightning is achievable across most of the globe, having crucial implications for our understanding of not only lightning, but also severe weather development, climate science, and more.**

***Index Terms*— Geolocation, lightning mapping, low-Earth orbit (LEO), radio frequency (RF), time of arrival (TOA).**

I. Introduction

LIGHTNING occurrence is directly tied to hydrometeor content and vertical wind motion within thunderstorms [1], [2], [3], [4], such that lightning can be used to identify the propensity of a convective system to produce severe weather [5], [6], [7]. Atmospheric chemical composition is influenced by lightning through the production of nitrogen oxides (NOx), which regulates atmospheric ozone and hydroxyl radical in the troposphere [8]. This supports the idea of a cycle in which increased ozone contributes to a warmer climate, increasing lightning rate, producing more ozone, and so on [9]. Hence, lightning measurements can improve both weather and climate forecasts (e.g., [10]). Moreover, because lightning is a distinctive signature of deep convection, it can be used to infer climatological changes in storm frequency and intensity—a signal that has become particularly sensitive at high latitudes [11], [12], [13].

Satellite-based optical lightning detectors have been used since the 1990s to map global lightning activity from the vantage point of low-Earth orbit (LEO) [14], [15] and more recently in geostationary orbit aboard the Geostationary Lightning Mapper (GLM) [16], [17], [18]. They provide 2-D maps of in-cloud (IC) and cloud-to-ground (CG) lightning flashes and are used to monitor weather and study the climate. A stereo mapping technique has been developed for 3-D geolocation of lightning and demonstrated within overlapping GLM fields of view [19]. This could also be accomplished with overlapping LEO-based optical lightning mappers, but this optical technique primarily provides a measure of cloud-top altitude and gives an obscured, 3-D view of the lightning channel geometry. A promising machine learning approach to estimate flash altitude from a single GLM sensor has also been developed [20]. It combines 2-D optical measurements from GLM with 3-D observations from a ground-based radio frequency lightning network to train a random forest model capable of retrieving the altitude of the charge layer where a GLM group originates. However, this approach is limited by the detection efficiency of optical lightning mappers, which can suffer in optical thick clouds and toward the edges of their field of view (e.g., [21], [22]).

Electrical breakdown associated with lightning activity also produces radio wave signals, which are insensitive to cloud scattering but can be affected by the ionosphere. The Fast On-orbit Recording of Transient Events (FORTE) satellite demonstrated that very high-frequency (VHF) radio receivers tunable between 20 and 300 MHz can be used to detect lightning activity from space. FORTE also carried an optical lightning detector that has been combined with its VHF detections to locate the altitude of lightning discharges [23]. This approach relies on the time delay between the direct and reflected VHF wave generated by lightning, often called a trans-ionospheric pulse pair (TIPP; [24]). Determining source altitudes using this method still requires coincident ground detection or optical observations. However, not all VHF events

Manuscript received 20 November 2023; revised 8 March 2024; accepted 1 April 2024. Date of publication 8 May 2024; date of current version 28 May 2024. This work was supported in part by NASA through a fellowship under the NASA Postdoctoral Program administered by Oak Ridge Associated Universities (first author's contribution) and in part by the NASA Earth Science Technology Office (coauthors contributions). The work of Sarah M. Stough was supported by the NASA Cooperative Agreement 80MSFC22M0001. *(Corresponding author: Jackson R. Remington.)*

Jackson R. Remington, Patrick N. Gatlin, and Timothy J. Lang are with the NASA Marshall Space Flight Center, Huntsville, AL 35812 USA (e-mail: jrremington1@gmail.com).

Sarah M. Stough is with the Cooperative Institute for Severe and High-Impact Weather Research and Operations (CIWRO), The University of Oklahoma, Norman, OK 73019 USA, and also with the National Severe Storms Laboratory, Norman, OK 73072 USA.

Nikhil Pailoor, Sonja A. Behnke, and Harald E. Edens are with Los Alamos National Laboratory, Los Alamos, NM 87545 USA.

Digital Object Identifier 10.1109/TGRS.2024.3398508

may have both a reflected wave and corresponding optical event—such coincidences are found for only 32% of the FORTE VHF triggers analyzed by [25], albeit physical and/or instrumental constraints can be a limiting factor (e.g., optically thick cloud, different spectral fingerprint, below detection threshold, and trigger rates).

A more detailed depiction of lightning activity is made with a lightning mapping array (LMA), which is a ground-based network of approximately ten radio-receiving stations that use a time-of-arrival (TOA) techniques and global positioning system (GPS) receivers to reconstruct the 3-D structure of lightning channels from VHF sources with high spatial and temporal resolution [26], [27]. The 3-D observations from such networks paint a greatly enhanced picture of lightning development within the cloud and how it is influenced by the fluxes of ice particles throughout the thunderstorm life cycle [5], [28], [29], [30], [31] as well as insights into volcanic eruptions [32] and constraints on the production of lightning NOx [33], [34], [35]. A major limitation of these ground-based VHF networks is their 3-D coverage, which for most LMAs is within 100 km from the network center and is restricted by line of sight [27], [36], [37], [38]. Hence, it is not practical to obtain 3-D maps of total (combined IC and CG) lightning activity on a global scale using ground-based networks. There is a need for a space-based capability.

The possibility and utility of similar multidetector TOA techniques have also been explored using GPS satellites [39], [40], [41]. The findings suggested that only the most powerful VHF emissions could be geolocated, perhaps limited by the high orbital altitudes of 20 000 km. However, FORTE has since reported a zoo of detectable features from LEO at an altitude of ~825 km while resolving the diurnal cycle [42]. In order to benefit from their closer proximity, remote-sensing instruments in LEO face additional limitations in the form of a restricted observation duration and latitude coverage only up to the orbital inclination.

One application of this quasi-global 3-D mapping capability is inferring the polarity of the main charge regions and estimating their altitudes and depths with high vertical resolution, which is important because they in turn map the distribution of charged hydrometeors by vertical motions within the cloud (e.g., [43], [44], [45], [46], [47]). Hence, the relative distance between charge layers is related to the storm lifecycle (e.g., [48]), and monitoring them can provide insights into the key processes that drive severe weather and potentially the cause of terrestrial gamma ray flashes and upper atmospheric electrical discharges (e.g., [43], [49], [50], [51]).

The feasibility of mapping charge structure from the vantage point of space has yet to be established—can a spaceborne VHF lightning mapping network locate 3-D sources with a 1–2 km accuracy needed to depict the gross electrical charge structure of a thunderstorm? How is geolocation accuracy affected by array geometry, increased attenuation, and dispersion when observing lightning RF signals from low-Earth orbit (LEO)? This study seeks to address these questions.

II. Methods

A. LMA Simulation Software and Modifications

Lightning observations from LMAs can be impacted by both detection efficiency and location accuracy at the VHF source and combined flash levels. Historically, Monte Carlo simulations, curvature matrix theory, and additional linearized methods have been employed to model LMA performance (e.g., [27], [36]). Python-based "LMAsimulation" software has been developed for standard ground-based LMAs to address location accuracy and detection efficiency through application of either Monte Carlo modeling or curvature matrix calculations and is adaptable to any unique network configuration with variable individual sensor performance characteristics [37]. In addition to quantifying the error associated with existing ground-based LMA configurations, its adaptability makes the software well-suited to inform the design of new LMA networks, including a space-based design concept.

To address the feasibility of an LMA-like constellation deployed in LEO, the LMAsimulation software was modified to transform a ground-based network to the space-based perspective. First, the original LMAsimulation software incorporates a tangent plane reference system to properly account for line-of-sight considerations owing to the Earth's curved surface, which limits the maximum range of lightning detection from the perspective of a ground-based network. As ground-based line-of-sight considerations do not similarly impact space-based observations, the LMAsimulation software was modified to exchange the tangent plane coordinate system with an Earth-centered, Earth-fixed (ECEF) coordinate system.

Additionally, a few minor source detection constraints were modified from the original LMAsimulation software for calculating VHF source location accuracy in space. Though time-of-arrival (TOA) methods technically require detections by at least four noncollocated sensors to determine the timing and 3-D location of a source, operational ground-based LMAs typically use ten or more stations and require at least six interdependent arrival time measurements to aid in distinguishing true lightning emission from noise and minimizing mislocations due to near-simultaneous observation of extraneous sources [26], [27]. However, fewer stations are desired for a spaceborne array (due to cost) and we relaxed the minimum number of required detections to between 4 and 6 VHF sensors in a LEO constellation. Because this study is focused on demonstrating the potential geolocation accuracy independently of detection efficiency, source power considerations were also decoupled from the simulation to ensure all sources were detected by each satellite. Further studies of these factors would be instrumental in determining the type and amount of sources that could be geolocated from LEO.

With space-based detection, there are three expected sources of geolocation error in the TOA algorithm: geometric effects based on the configuration of satellites relative to VHF sources, ionospheric effects including RF signal dispersion and the "dechirping" process (Section II-C), and instrumental uncertainties. This study aims to determine the effect

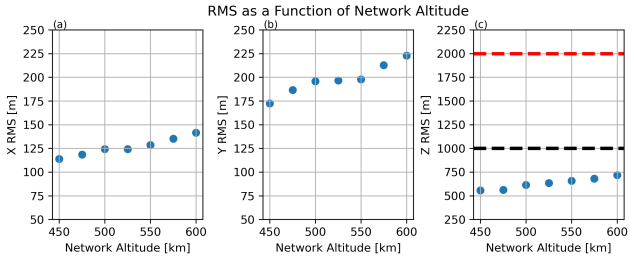

Fig. 1. Root mean square error calculated for (a) x-coordinate (East–West), (b) y-coordinate (North–South), and (c) z-coordinate (altitude) of simulated VHF source locations over a range of simulated network altitudes in low-Earth orbit. For each simulated network altitude, 1000 sources at 7 km altitude were simulated at the geographic center of the simulated network with horizontal spacing of 400 km. Blue markers indicate the rms errors produced by the simulations while ignoring atmospheric effects.

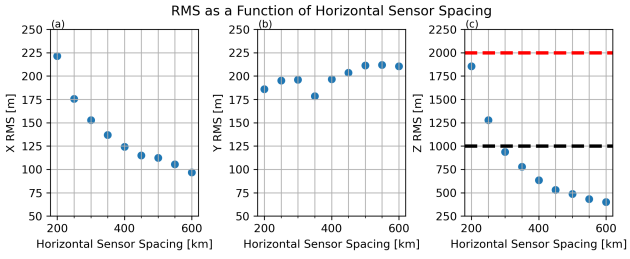

Fig. 2. Root mean square error calculated for (a) x-coordinate (East–West), (b) y-coordinate (North–South), and (c) z-coordinate (altitude) of simulated VHF source locations using constellations with a range of horizontal spacing distances. For each spacing distance, 1000 sources at 7 km altitude were simulated at the geographic center of the simulated network with an orbital altitude of 525 km. Blue markers indicate the rms errors produced by the simulations while ignoring atmospheric effects.

of these errors on overall source location accuracy for a generalized constellation of satellites. As such, topics which are largely hardware dependent (e.g., detection threshold) are not addressed. On the other hand, instrumental timing error is necessary for realistic geolocation simulations and can be conservatively estimated based on existing ground and space-based sensors. For this study with many stations moving at high speeds, a conservative rms error of 100 ns was used, as compared to approx. 23–46 ns in studies of stationary, ground-based LMA stations [27], [37].

B. Array Geometry

Basic versions of this simulation were run initially without considering ionospheric effects while developing the constellation configuration. Altitude and satellite spacing were varied at a range of latitudes while simulating an idealized VHF source directly below the array center. Fig. 1 shows the relationship between constellation altitude and resulting location accuracy around the chosen altitude of 525 km, highlighting their weak interdependence in LEO. Other considerations could be made based on instrumentation or preferred orbit, but this choice was largely arbitrary for this concept study. The horizontal separation between stations, however, has a much stronger effect on geolocation accuracy, particularly in the vertical. Fig. 2 shows that average errors are lower for more spread-out constellations, but at a cost. These TOA analyses require as many redundant detections as possible, and a source is more likely to be detected by several satellites when they are closer together. The constellation was thus designed to consist of two orbital planes with inclinations near $\simeq 62°$, each having three stations separated by 300 km, minimizing horizontal spacing while keeping vertical accuracy under 1 km for an idealized source at nadir.

Fig. 3 illustrates how these orbital planes affect array geometry across a limited range of latitudes. At 60°N for example (top row), the two orbits converge, reducing their horizontal spacing and increasing perpendicular rms errors. Because the spacing along each orbit remains constant, errors parallel to the orbit direction are fairly consistent at each latitude (left column). Note that the simulations of Fig. 3 represent an initial step informing the orbital configuration development alongside Figs. 1 and 2, and should not be compared directly to later results. They were run with symmetrical

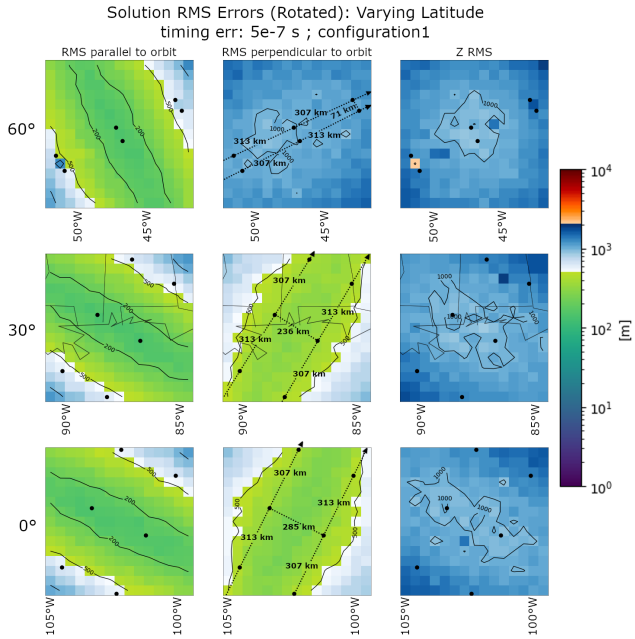

Fig. 3. Root mean square error calculated for x' coordinate (parallel to orbit path, left column), y' coordinate (perpendicular to orbit path, middle column), and z coordinate (right column) of simulated VHF source locations at (bottom row) low, (middle row) middle, and (top row) high latitudes in a grid underneath the original, symmetric satellite configuration described in Section II-B (black dots). Dimensions of the configuration at each latitude are shown in the middle column with arrows indicating the orbit direction. The error colorbar transitions at 500 and 2000 m to highlight those specific value ranges with labeled contours in black. Note that these simulations were run with the original, symmetric configuration during development, use a higher assumed instrumental timing error of 500 ns, and do not include any ionospheric effects.

satellite spacing, no ionospheric effects, and assumed a higher instrumental timing error of 500 ns. Satellite positions along each orbital path were later varied to avoid symmetry between individual baselines in the array while maintaining the 300 km average separation distance (see Section III-B). The original and adjusted configurations are compared in Section III to help illustrate the geometric effects of geolocation accuracy.

In addition to the satellites' orbital positions, geometric effects also include varying number of stations. This is standard practice for simulating LMAs of different sizes, with a well-defined LMA event defined as being detected by a minimum of six ground stations (Section II-A). Cost and

instrument size are much more restrictive in the case of an orbiting array, however, and therefore it becomes increasingly vital to evaluate the performance of smaller constellations with the possibility of fewer than six minimum detections. For example, signal power loss due to dispersive and range effects may prevent signal detection by one or more satellites. In these cases, a system with more flexible minimum conditions may still be able to reconstruct 3-D source locations, albeit with increased uncertainty.

Although outside the scope of this analysis, it is worth noting that this minimum could be extended below four satellites with the addition of alternative detection methods to provide redundant measurements. For example, two coordinates could be provided by an onboard optical imager, the most common type of orbital lightning detector, constraining both horizontal coordinates (x, y) with resolution depending on pixel size (e.g., [14], [15], [16]). This would leave the two remaining coordinates of time and altitude (t, z) to be solved by TOA analysis using the time of detected RF signals as above. In contrast to these techniques is the single-satellite approach taken by FORTE [23], which provided both optical and RF measurements of lightning flashes to account for the x, y, and t coordinates. The fourth crucial measurement z was made in the form of Earth-reflected pulses as introduced in Section I. These four measurements then give a well-determined solution to the four coordinates with reasonable vertical resolution. The downsides of this approach are its reliance on detecting coincident optical and reflected pulses [25], [52], [53], [54].

C. Ionospheric Model

An LMA in LEO must also detect VHF sources through the depth of Earth's atmosphere, including the ionosphere, which uniquely impacts electromagnetic propagation. A robust model of ionospheric effects was applied accordingly to more accurately simulate VHF emission and propagation. These simulations use a double exponential function to emulate a burst of VHF lightning emission at 10 km altitude with an impulsive signature. The ionosphere is modeled as a slab of uniform electron density. An input vertical total electron count (vTEC) representing the ionosphere's integrated electron density along a vertical path is converted to slant TEC by assuming uniform electron density and applying the signal's travel path length through the ionosphere. For this study, we used vertically integrated TEC values of 5, 30, and 60 (in units of TECU $= 10^{16}$ electrons/m^2) to sample diurnal, seasonal, and solar cycle variations. These values do not reflect the full range of global ionospheric vTEC, but are fairly representative of the simulated mid-latitude region centered at 30.2°N, 92.3°W [55]. For comparison, Data of the International Global Navigation Satellite System Global Ionospheric Maps (IGSG), available via Earthdata.nasa.gov, report average day (night) vTEC values of 12 (8) TECU at periods of low solar activity and 37 (17) TECU at periods of high solar activity, though mid-day peaks at this latitude occasionally reach 60 TECU and above. Near the magnetic equator during solar maximum, these peaks can even exceed 100 TECU. Conversely, vTEC typically remains below 10–20 TECU at night and at high latitudes.

The dispersion of VHF signals was forward-modeled using the full Appleton–Hartree equation [56], [57], [58], [59] following the example of [60]. Refraction was handled by satisfying Snell's law for each frequency at the ionosphere's boundaries. Birefringence was accounted for by calculating wave polarization using available magnetic field orientations obtained from International Geomagnetic Reference Field data (IGRF; [61]). A single, unpolarized plane wave incident on a border of ionospheric plasma can be decomposed into two modes of forward propagating waves (plus two backward-propagating waves). These were traced individually at each frequency and resulted in two circularly polarized modes arriving at each orbiting station. All frequencies and modes were then recombined, producing a properly dispersed waveform.

In order to realistically simulate the potential of calculating a source's time of arrival, we processed this waveform in a way that emulates a physical detector. We first combined the dispersed, 3-D vector electric field into right-hand circular polarization to suppress one of the birefringent wave modes. We then added Gaussian noise to achieve a signal-to-noise power ratio of 10:1. Although this power ratio is lower than the subband threshold used by FORTE [23], it is used only to introduce noisy signal dithering and does not affect the detectability in these simulations. We artificially sampled the result at 200 megasamples/s, then applied a 40–60 MHz bandpass filter to capture and isolate the targeted frequency range using a direct-digitization approach.

The processed signal was then dechirped by finding the TEC value that maximizes kurtosis of the time-series waveform (e.g., [23]). The peak of the dechirped signal was defined as the simulated time of arrival at each station. This process only accounts for first-order dispersion effects that are proportional to the electron density and does not remove all of the dispersion. As such, the residual error in the arrival times, which varies over the constellation, is one of the main contributors to geolocation accuracy. Further dispersion removal due to magnetic field effects is possible once an initial solution for the location is known. These arrival times were further varied according to a normal distribution with standard deviation equal to the assumed instrumental timing error of 100 ns, based on the current capability of commercial Global Navigation Satellite System (GNSS) receivers for small satellite applications (e.g., [62]).

III. Results and Discussion

The simulations outlined above in Section II were run using generated sources spread over a 600 × 600 km square centered on the constellation's nadir to determine the uncertainty of reconstructed coordinates and produce the plots of this section. Results are given in a rotated coordinate frame as parallel and perpendicular to the constellation's orbital path (dubbed x' and y', respectively). Simulations were performed at mid-latitude (30.2°N, 92.3°W) with source altitudes of 10 km and do not consider source power, instrument design, nor the resulting detection efficiency. These excluded factors have particular influence on any sources originating from outside the 360 000 km^2 region examined here. Strong lightning emissions from farther away will still be detectable if their power is

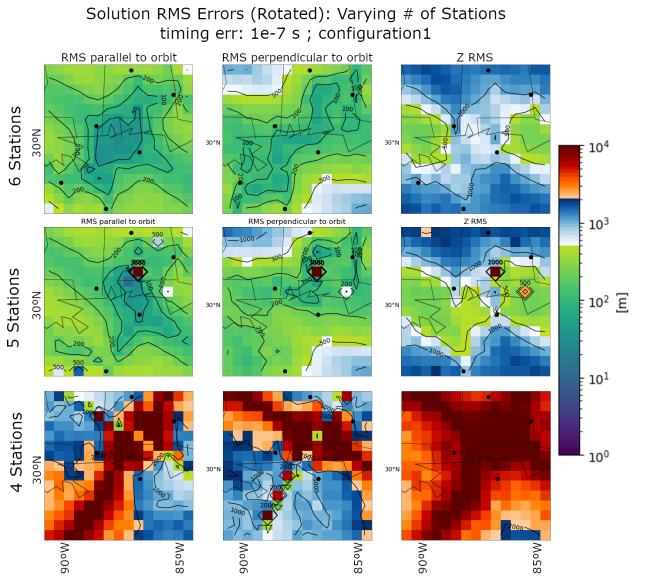

Fig. 4. Root mean square error calculated for x' coordinate (parallel to orbit path, left column), y' coordinate (perpendicular to orbit path, middle column), and z coordinate (right column) of 250 simulated VHF sources at each grid point underneath the original, symmetric orbital configuration described in Section II-B. The configuration contains 6, 5, and 4 satellites in the respective top, middle, and bottom rows with locations displayed as the overlaid black dots. These simulations were run at 30° latitude and with a 30 vTEC ionosphere. The colorbar transitions at 500 and 2000 m to highlight those specific value ranges.

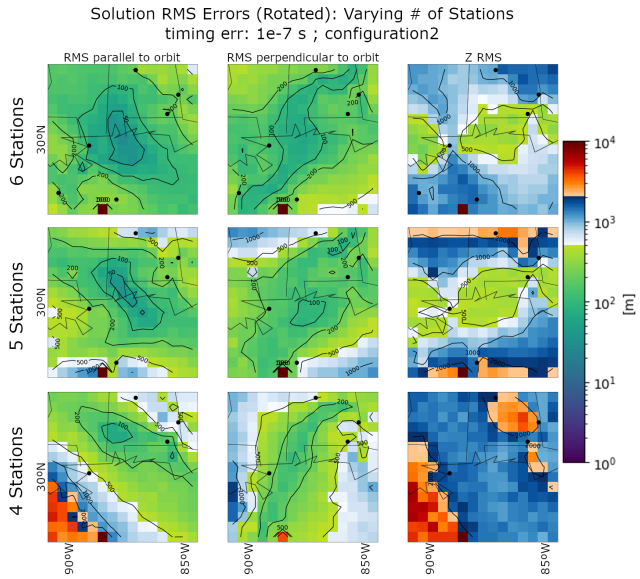

Fig. 5. Same as Fig. 4, but for the adjusted orbital configuration with reduced symmetry as described in Section II-B. Dimensions of this configuration are shown in Fig. 6 for clarity.

high enough to surpass instrument thresholds, but would be poorly geolocated and may also interfere with those of closer sources if observed near-simultaneously. In practice, satellite receivers may be able to identify and discard these signals based on their greater signal dispersion or using complex antenna geometries [63]. However, since it has been shown that the observation rate of near-simultaneous, strong IC pulses by space-based platforms is relatively low [64], these results focus on the geolocation of temporally isolated emissions.

A. Geometric Effects

Figs. 4 and 5 show the resulting rms errors when varying the number of active satellites in the original symmetric and modified constellation configurations, respectively. These simulations were run under the same ionospheric conditions with electron density of 30 vTEC to isolate geometric variations. Quantitatively, the average geolocation errors for the original six-satellite configuration (top row of Fig. 4) were 180, 280, and 940 m for the x', y', and z coordinates, respectively. The five-satellite location errors (middle row) were comparable at 230, 330, and 910 m. Surprisingly, the average vertical error here is slightly lower than for six satellites, especially at the array center. We speculate that this is due to the reduced symmetry of the five-satellite configuration for central sources, resulting in fewer local minima in the geolocation algorithm. Outside the array's footprint, accuracy drops off more quickly for five satellites, hence the average error would likely be higher than for six satellites if a larger field of view were considered.

For the well-determined solutions using four satellites, while technically containing the necessary number of measurements, there are zero degrees of freedom to compensate for inherently noisy observations. This produces inconsistent solutions with average errors exceeding several kilometers (bottom row). As explored in Sections I and II, the poor resolution and coverage of this result could theoretically be remedied by including a 2-D imager onboard one or more satellites to constrain sources' horizontal positions in the minimization algorithm, but would require correlated optical emissions. Using only RF observations, however, four-satellite solutions are largely unreliable while five- or six-satellite solutions can geolocate sources within the 1–2 km accuracy preferred for mapping thunderstorm charge structures.

One feature of note across many of these results is the occasional grid point with much higher error than those surrounding it (e.g., middle row of Fig. 4). These poor solutions are likely a result of shallow gradients in the minimization algorithm and typically occur at the midpoint between two or more satellites. This was one factor leading to the satellite configuration's redesign to minimize baseline symmetry. However, the features can still occur as in Fig. 5, depending not only on array geometry but also on local ionospheric conditions.

For the altered configuration of Fig. 5, contour plots show the subtle changes that accompany shifting satellite positions while the overall errors are slightly lower than those of the original configuration. With six active satellites, average errors are 160, 210, and 850 m for the x', y', and z coordinates. The 3-D resolution of individual sources is <2 km for the entire 360 000 km^2 region beneath the constellation, producing a swath ≥ 600 km wide trailing behind the orbit over mid-latitudes with accuracy sufficient for determining charge structure. This contains a smaller region of 216 000 km^2 with 3-D resolution <1 km (approx. 530 km swath width). With this asymmetric configuration using five active satellites, average errors are somewhat higher for each respective coordinate axis at 290, 330, and 1100 m. Three-dimensional source resolution is <2 km for approx. 88% of the analyzed area,

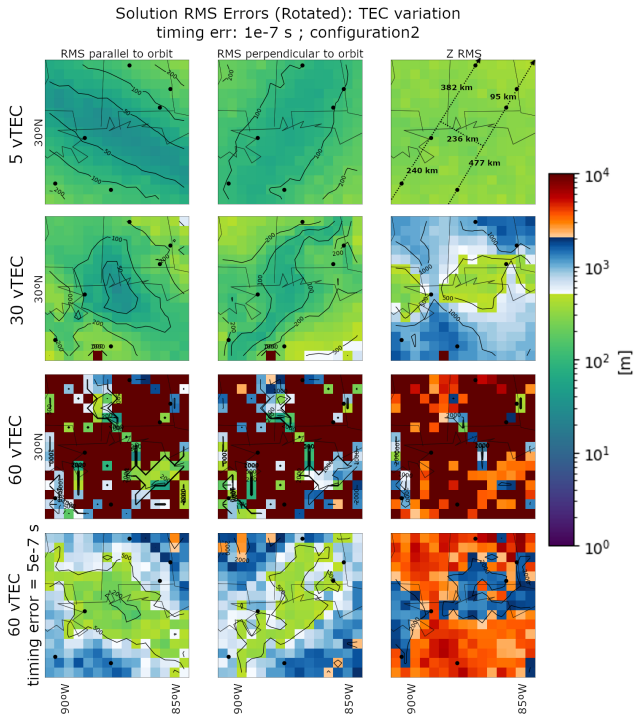

Fig. 6. Same as Fig. 5, but with varying simulated ionospheric vTEC values of (top row) 5, (second row) 30, and (third row) 60. The fourth row also shows 60 vTEC, but with a higher instrumental timing error of 500 ns in order to improve the poor convergence rates seen in the row above. These simulations were run with six satellites in the altered orbital configuration with reduced symmetry. The altered horizontal spacing between and along each orbit are shown in the top right panel for clarity with arrows indicating orbit direction.

covering 315 000 km^2 (again $\geq$600 km swath width). Coverage with $<$1 km resolution is $\simeq$160 000 km^2, equivalent to 450 km swath width. The bottom row again shows the inaccuracy and inconsistency of four-satellite solutions, having average errors of 760, 500, and 2000 m.

For those solutions which were overdetermined (involving $\geq$5 detections), the resulting curvature matrices were also calculated and inverted as an alternative method of approximating each coordinate's error and saving on computation time as described in [36] and [37]. However, these are a metric of array geometry and instrumental errors, ignoring ionospheric effects and resulting in plots nearly identical to those with 5 vTEC in Fig. 6. For this study, it was perfectly feasible to use the more thorough statistical rms location errors above to illustrate all sources of uncertainty.

B. Ionospheric Effects

Fig. 6 shows the resulting errors of the six-satellite configuration under varying ionospheric conditions of 5, 30, and 60 vTEC values. Empirically, the 5 vTEC solutions are a good visualization of purely geometric effects with negligible ionospheric influence. Namely, gradients in horizontal accuracy are oriented along their respective coordinates while vertical accuracy remains nearly flat. With increasing vTEC, these patterns are warped by the effect of dispersion on signal arrival times. At 60 vTEC, the geolocation algorithm fails to converge on many source locations, particularly beneath satellite positions. Including higher order corrections in the dechirping algorithm would improve overall accuracy and convergence rate. Interestingly, if the instrumental timing error is relaxed from 100 to 500 ns as in the bottom row of Fig. 6, the first-order-corrected arrival times are usually dithered enough to determine source locations that otherwise failed to converge, albeit with poor accuracy. The plots of this bottom row using 500 ns are not a direct comparison to those above, but they nevertheless demonstrate that the geolocation algorithm can be adapted to improve convergence rates over regions with high ionospheric electron density and still determine at least horizontal coordinates with $<$1 km resolution.

As expected, quantitative rms errors were significantly lower for 5 vTEC than the 30 vTEC solutions above: 85, 113, and 292 m for their respective x', y', and z coordinates. Relative to mid-latitudes, 60 vTEC represents an atypically high ionospheric density, resulting in mostly failed solutions. Those that converged had average errors of 610, 870, and 2400 m, outside the 1–2 km range for reliably determining charge structure. When 60-vTEC simulations were run with higher timing uncertainty, convergence rates recovered but resulted in slightly higher average errors of 720, 870, and 2700 m. Only 28% of the area analyzed produced source solutions with $<$2 km 3-D resolution (approx. 100 000 km^2 or 360 km swath width).

Again, note that these vTEC samples represent low to high ionospheric conditions of this mid-latitude region, but do not cover the high peaks close to the magnetic equator where RF-based geolocation becomes increasingly difficult. Conversely, better accuracy and reliability would be expected at night and high latitudes where vTEC values remain below 10–20 TECU for extended periods of time.

IV. Conclusion

Together, the results above demonstrate the feasibility of geolocating lightning sources using RF-only TOA methods with $<$1–2 km rms error in all three spatial dimensions across large swaths of the globe. The 3-D geolocation accuracy from this LEO simulation varies with latitude and is sensitive to the number and relative configuration of the satellites within the constellation (i.e., geometry) as well as the ionospheric variability. At mid-latitudes and for an ionosphere characterized by an electron density of 30 vTEC, we find five satellites are sufficient to achieve $<$2 km rms error in VHF source altitude over 525 km swaths under the constellation. This coverage increases by at least 12% at mid-latitudes with an additional satellite. Source locations at this resolution are sufficient for mapping 3-D flash locations and cloud charge structures. These potential measurements can support meteorological and hydrological studies by monitoring vertical wind motion, precipitation, and intensification of thunderstorms [3], [6], [7], [11]. Even finer vertical resolution ($<$1 km) is achievable for a smaller region within this swath ($\sim$50% with five satellites), which suggests that mapping small-scale flash structure is a possibility. In addition to its value in isolating updraft regions within convective storms (e.g., [65]), this level of resolution would facilitate a more robust depiction of LNOx production (e.g., [35]) on a global scale. That being said, mapping flash channel and charge

structure accurately requires detecting enough VHF sources throughout flash development. Further study is necessary to determine the sensitivity of such an instrument. The subject is already being explored and may provide insight on the amount and types of lower power VHF emissions that would be detectable from LEO [66]. Even under conditions where mapping channel structure with 1 km accuracy is not possible, the coarser VHF source altitude can still yield estimates of LNOx profiles with sufficient resolution to constrain chemical transport models (e.g., [67]).

The relative arrangement of VHF receivers in LEO affects both the size and shape of high-resolution coverage, similar to an LMA network (e.g., [68]). Unlike LMAs, however, the effective 3-D coverage of a satellite constellation is not constant and varies with latitude. The spacing between satellites in each orbit can be altered to reduce symmetry and improve the TOA algorithm's consistency. Optimizing constellation formation is nontrivial, and special care should therefore be taken to ensure geolocation fidelity throughout the chosen orbit.

Ionospheric effects are shown to be the main contributors to average geolocation error and consistency. The 3-D retrievals are most accurate when electron density is low (e.g., at night or during solar minimum), but lose reliability over medium to high TEC values. Results of Section II-C show that an increase from 30 to 60 vTEC effectively reduces the coverage of <2 km resolution by nearly 72%. During these conditions, the geolocation algorithm begins failing to converge on solutions, though considering higher order effects in the dechirping process (e.g., magnetic field orientation with respect to direction of wave propagation) would improve this performance overall. Results presented in Section II-C also suggest that instrumental timing error could be artificially relaxed to increase convergence rates during high-TEC conditions and retain 2-D horizontal accuracy better than 1 km.

Lightning has now been classified as an essential climate variable by the World Meteorological Organization [69] and needs to be a focus in the coming decade to complement and support the future of atmospheric science missions like the Atmospheric Observing System (AOS) and Investigation of Convective Updrafts (INCUS). Even so, the Lightning Imaging Sensor (LIS) has been removed from the International Space Station in late 2023, leaving a gap in meteorological observation that can and should be filled by instruments that can expand our current capabilities. For example, the advantages of this VHF-only detection method are not only its reliable altitude determination, but also its potential to map out lightning flash structure regardless of cloud cover or visibility, an advantage typically reserved for ground-based arrays with small areas of coverage. In addition to lowering the necessary number of satellites for TOA geolocation by constraining horizontal flash locations, and as noted by [70], complementary on-board optical imagers would grant further insight and capture a more complete picture of lightning activity. In essence, an orbital, TOA-based method of 3-D lightning mapping would unlock a treasure trove of information needed to improve our understanding of global thunderstorms and their effects on the surrounding environment.

ACKNOWLEDGMENT

The authors would like to thank the Science Research and Projects Office at NASA Marshall Space Flight Center (MSFC) for supporting the constellation design component of this work, and Randy Hopkins at MSFC for providing the orbit data from that study. They also thank Vanna Chmielewski for her work developing the LMAsimulation software and guidance for modifying it. They sincerely appreciate the Reviewers' thoughtful comments and recommendations which helped improve the quality of the paper.

REFERENCES

[1] D. R. MacGorman and W. D. Rust, *The Electrical Nature of Storms*. London, U.K.: Oxford Univ. Press, 1998.

[2] E. R. Williams, M. E. Weber, and R. E. Orville, "The relationship between lightning type and convective state of thunderclouds," *J. Geophys. Res., Atmos.*, vol. 94, no. D11, pp. 13213–13220, Sep. 1989.

[3] T. J. Lang and S. A. Rutledge, "Relationships between convective storm kinematics, precipitation, and lightning," *Monthly Weather Rev.*, vol. 130, no. 10, pp. 2492–2506, Oct. 2002.

[4] W. Deierling and W. A. Petersen, "Total lightning activity as an indicator of updraft characteristics," *J. Geophys. Res., Atmos.*, vol. 113, no. D16, Aug. 2008, doi: 10.1029/2007JD009598.

[5] E. Williams et al., "The behavior of total lightning activity in severe Florida thunderstorms," *Atmos. Res.*, vol. 51, nos. 3–4, pp. 245–265, Jul. 1999.

[6] P. N. Gatlin and S. J. Goodman, "A total lightning trending algorithm to identify severe thunderstorms," *J. Atmos. Ocean. Technol.*, vol. 27, no. 1, pp. 3–22, Jan. 2010.

[7] C. J. Schultz, L. D. Carey, E. V. Schultz, and R. J. Blakeslee, "Kinematic and microphysical significance of lightning jumps versus nonjump increases in total flash rate," *Weather Forecasting*, vol. 32, no. 1, pp. 275–288, Feb. 2017.

[8] L.T. Murray, "Lightning NO_x and impacts on air quality," *Current Pollut. Rep.*, vol. 2, p. 115–133, Jan. 2016.

[9] U. Schumann and H. Huntrieser, "The global lightning-induced nitrogen oxides source," *Atmos. Chem. Phys.*, vol. 7, no. 14, pp. 3823–3907, Jul. 2007.

[10] C. G. Price, "Lightning applications in weather and climate research," *Surv. Geophys.*, vol. 34, no. 6, pp. 755–767, Nov. 2013.

[11] E.R. Williams, "Lightning and climate change," in *Lightning Interaction With Power Systems: Fundamentals and Modelling*. London, U.K.: Institution of Engineering and Technology, 2020, pp. 1–45.

[12] R.H. Holzworth, "Lightning in the Arctic," *Geophys. Res. Lett.*, vol. 48, Apr. 2021, Art. no. e2020GL091366.

[13] D. Kępski and M. Kubicki, "Thunderstorm activity at high latitudes observed at manned WMO weather stations," *Int. J. Climatol.*, vol. 42, no. 15, pp. 7794–7816, Dec. 2022.

[14] H. J. Christian et al., "Global frequency and distribution of lightning as observed from space by the optical transient detector," *J. Geophys. Res., Atmos.*, vol. 108, no. D1, pp. ACL 4-1–ACL 4-15, Jan. 2003.

[15] R. J. Blakeslee et al., "Three years of the lightning imaging sensor onboard the international space station: Expanded global coverage and enhanced applications," *J. Geophys. Res., Atmos.*, vol. 125, no. 16, Aug. 2020, Art. no. e2020JD032918.

[16] S. J. Goodman et al., "The GOES-R geostationary lightning mapper (GLM)," *Atmos. Res.*, vols. 125–126, pp. 34–49, May 2013.

[17] D. Cao, F. Lu, X. Zhang, and J. Yang, "Lightning activity observed by the FengYun-4A lightning mapping imager," *Remote Sens.*, vol. 13, no. 15, p. 3013, Jul. 2021.

[18] S.-E. Enno, B. Viticchiè, and J. Grandell, "Meteosat third generation lightning imager for the continuous monitoring of lighting from space," in *Proc. 11th Eur. Conf. Severe Storms*, Bucharest, Romania, May 2023, doi: 10.5194/ecss2023-135.

[19] D. Mach and K. Virts, "A technique for determining three-dimensional storm cloud-top locations using stereo optical lightning pulses observed from orbit," *J. Atmos. Ocean. Technol.*, vol. 38, pp. 1993–2001, Nov. 2021.

[20] M. Peterson, T. E. L. Light, and D. Mach, "The illumination of thunderclouds by lightning: 3. Retrieving optical source altitude," *Earth Space Sci.*, vol. 9, no. 1, Jan. 2022, Art. no. e2021EA00194.

[21] S. A. Rutledge, K. A. Hilburn, A. Clayton, B. Fuchs, and S. D. Miller, "Evaluating geostationary lightning mapper flash rates within intense convective storms," *J. Geophys. Res., Atmos.*, vol. 125, no. 14, Jul. 2020, Art. no. e2020JD03282.

[22] M. Bateman, D. Mach, and M. Stock, "Further investigation into detection efficiency and false alarm rate for the geostationary lightning mappers aboard GOES-16 and GOES-17," *Earth Space Sci.*, vol. 8, no. 2, Feb. 2021, Art. no. e2020EA00123.

[23] A. R. Jacobson, S. O. Knox, R. Franz, and D. C. Enemark, "FORTE observations of lightning radio-frequency signatures: Capabilities and basic results," *Radio Sci.*, vol. 34, no. 2, pp. 337–354, Mar. 1999.

[24] R. S. Massey and D. N. Holden, "Phenomenology of transionospheric pulse pairs," *Radio Sci.*, vol. 30, no. 5, pp. 1645–1659, Sep. 1995.

[25] T. E. L. Light and A. R. Jacobson, "Characteristics of impulsive VHF lightning signals observed by the FORTE satellite," *J. Geophys. Res., Atmos.*, vol. 107, no. D24, pp. ACL 8-1–ACL 8-8, Dec. 2002.

[26] W. Rison, R. J. Thomas, P. R. Krehbiel, T. Hamlin, and J. Harlin, "A GPS-based three-dimensional lightning mapping system: Initial observations in central new Mexico," *Geophys. Res. Lett.*, vol. 26, no. 23, pp. 3573–3576, Dec. 1999.

[27] R. J. Thomas et al., "Accuracy of the lightning mapping array," *J. Geophys. Res., Atmos.*, vol. 109, no. D14, Jul. 2004.

[28] T. J. Lang et al., "The severe thunderstorm electrification and precipitation study," *Bull. Amer. Meteorolog. Soc.*, vol. 85, no. 8, pp. 1107–1126, Aug. 2004.

[29] W. Deierling, W. A. Petersen, J. Latham, S. Ellis, and H. J. Christian, "The relationship between lightning activity and ice fluxes in thunderstorms," *J. Geophys. Res., Atmos.*, vol. 113, no. D15, Aug. 2008, doi: 10.1029/2007JD009700.

[30] K. M. Calhoun, D. R. MacGorman, C. L. Ziegler, and M. I. Biggerstaff, "Evolution of lightning activity and storm charge relative to dual-Doppler analysis of a high-precipitation supercell storm," *Monthly Weather Rev.*, vol. 141, no. 7, pp. 2199–2223, Jul. 2013.

[31] P. Borque, "Distinctive signals in 1-min observations of overshooting Tops and lightning activity in a severe supercell thunderstorm," *J. Geophys. Res., Atmos.*, vol. 125, Aug. 2020, Art. no. e2020JD03285.

[32] S. A. Behnke et al., "Investigating the origin of continual radio frequency impulses during explosive volcanic eruptions," *J. Geophys. Res., Atmos.*, vol. 123, no. 8, pp. 4157–4174, Apr. 2018.

[33] T. C. Davis, S. A. Rutledge, and B. R. Fuchs, "Lightning location, NO_x production, and transport by anomalous and normal polarity thunderstorms," *J. Geophys. Res., Atmos.*, vol. 124, no. 15, pp. 8722–8742, Aug. 2019.

[34] I. B. Pollack et al., "Airborne quantification of upper tropospheric NO_x production from lightning in deep convective storms over the United States great plains," *J. Geophys. Res., Atmos.*, vol. 121, no. 4, pp. 2002–2028, Feb. 2016.

[35] W. Koshak, H. Peterson, A. Biazar, M. Khan, and L. Wang, "The NASA lightning nitrogen oxides model (LNOM): Application to air quality modeling," *Atmos. Res.*, vols. 135–136, pp. 363–369, Jan. 2014.

[36] W. J. Koshak et al., "North Alabama lightning mapping array (LMA): VHF source retrieval algorithm and error analyses," *J. Atmos. Ocean. Technol.*, vol. 21, no. 4, pp. 543–558, Apr. 2004.

[37] V. C. Chmielewski and E. C. Bruning, "Lightning mapping array flash detection performance with variable receiver thresholds," *J. Geophys. Res., Atmos.*, vol. 121, no. 14, pp. 8600–8614, Jul. 2016.

[38] B. R. Fuchs, E. C. Bruning, S. A. Rutledge, L. D. Carey, P. R. Krehbiel, and W. Rison, "Climatological analyses of LMA data with an open-source lightning flash-clustering algorithm," *J. Geophys. Res., Atmos.*, vol. 121, no. 14, pp. 8625–8648, Jul. 2016.

[39] D. M. Suszcynsky and M. J. Heavner, "Narrow bipolar events as indicators of thunderstorm convective strength," *Geophys. Res. Lett.*, vol. 30, no. 17, Sep. 2003, doi: 10.1029/2003GL017834.

[40] D. M. Suszcynski, K. C. Weins, and A. Jacobson, "VHF lightning detection and storm tracking from GPS orbit," in *Proc. 12th Conf. Aviation Range Aerosp. Meteorol.*, 2006. [Online]. Available: https://ams.confex.com/ams/Annual2006/techprogram/paper_105351.htm

[41] A. R. Jacobson and M. J. Heavner, "Comparison of narrow bipolar events with ordinary lightning as proxies for severe convection," *Monthly Weather Rev.*, vol. 133, no. 5, pp. 1144–1154, May 2005.

[42] S. M. Davis, D. M. Suszcynsky, and T. E. L. Light, "FORTE observations of optical emissions from lightning: Optical properties and discrimination capability," *J. Geophys. Res., Atmos.*, vol. 107, no. D21, pp. ACL 9-1–ACL 9-5, 2002, doi: 10.1029/2002JD002434.

[43] K. C. Wiens, S. A. Rutledge, and S. A. Tessendorf, "The 29 June 2000 supercell observed during STEPS. Part II: Lightning and charge structure," *J. Atmos. Sci.*, vol. 62, no. 12, pp. 4151–4177, Dec. 2005.

[44] B. L. Medina, L. D. Carey, T. J. Lang, P. M. Bitzer, W. Deierling, and Y. Zhu, "Characterizing charge structure in central Argentina thunderstorms during RELAMPAGO utilizing a new charge layer polarity identification method," *Earth Space Sci.*, vol. 8, no. 8, Aug. 2021, Art. no. e2021EA001803.

[45] S. M. Stough and L. D. Carey, "Observations of anomalous charge structures in supercell thunderstorms in the southeastern united states," *J. Geophys. Res., Atmos.*, vol. 125, no. 17, Sep. 2020, Art. no. e2020JD03301.

[46] S. A. Tessendorf, S. A. Rutledge, and K. C. Wiens, "Radar and lightning observations of normal and inverted polarity multicellular storms from STEPS," *Monthly Weather Rev.*, vol. 135, no. 11, pp. 3682–3706, Nov. 2007.

[47] D. R. MacGorman et al., "TELEX the thunderstorm electrification and lightning experiment," *Bull. Amer. Meteorolog. Soc.*, vol. 89, no. 7, pp. 997–1014, Jul. 2008.

[48] E. C. Bruning, W. D. Rust, D. R. MacGorman, M. I. Biggerstaff, and T. J. Schuur, "Formation of charge structures in a supercell," *Monthly Weather Rev.*, vol. 138, no. 10, pp. 3740–3761, Oct. 2010.

[49] J. A. López et al., "Charge structure of two tropical thunderstorms in Colombia," *J. Geophys. Res., Atmos.*, vol. 124, no. 10, pp. 5503–5515, May 2019.

[50] N. Pineda, T. Rigo, J. Montany, and O. A. van der Velde, "Charge structure analysis of a severe hailstorm with predominantly positive cloud-to-ground lightning," *Atmos. Res.*, vols. 178–179, pp. 31–44, Sep. 2016.

[51] G. Lu, "Coordinated observations of sprites and in-cloud lightning flash structure," *J. Geophys. Res., Atmos.*, vol. 118, pp. 6607–6632, Jun. 2013.

[52] R. S. Massey, D. N. Holden, and X.-M. Shao, "Phenomenology of transionospheric pulse pairs: Further observations," *Radio Sci.*, vol. 33, no. 6, pp. 1755–1761, Nov. 1998.

[53] A. R. Jacobson, K. L. Cummins, M. Carter, P. Klingner, D. Roussel-Dupré, and S. O. Knox, "FORTE radio-frequency observations of lightning strokes detected by the national lightning detection network," *J. Geophys. Res., Atmos.*, vol. 105, no. D12, pp. 15653–15662, Jun. 2000.

[54] M. Peterson, "FORTE measurements of global lightning altitudes," *Earth Space Sci.*, vol. 9, no. 9, Sep. 2022, Art. no. e2022EA002404.

[55] G. Johnston, A. Riddell, and G. Hausler, "The international GNSS service," in *Springer Handbook of Global Navigation Satellite Systems*, P. Teunissen and O. Montenbruck, Eds. Berlin, Germany: Springer, 2017, pp. 967–982.

[56] D. G. Swanson, "Plasma waves," in *Plasma Physics and Controlled Fusion*, vol. 45, 2nd ed. San Diego, CA, USA: Academic, 2003, pp. 10–69, doi: 10.1088/0741-3335/45/6/701.

[57] K. G. Budden, *Radio Waves Ionosphere*. Cambridge, U.K.: Cambridge Univ. Press, 1961.

[58] K. G. Budden, *The Propagation of Radio Waves: The Theory of Radio Waves of Low Power in the Ionosphere and Magnetosphere*. Cambridge, U.K.: Cambridge Univ. Press, 1985.

[59] K. C. Yeh, C. H. Liu, and S. R. Seshadri, "Theory of ionospheric waves," *IEEE Trans. Plasma Sci.*, vol. PS-1, no. 2, p. 42, Jun. 1973.

[60] M.E. Light, "Trans-ionospheric signal polarization," Los Alamos Nat. Lab., Los Alamos, NM, USA, Tech. Rep. LA-UR-21-20674, 2021, doi: 10.2172/1762727.

[61] P. Alken, E. Thébault, C. D. Beggan, and M. Nosé, "Special issue 'international geomagnetic reference field: The thirteenth generation," *Earth, Planets Space*, vol. 74, no. 1, Dec. 2022.

[62] C. Ruf et al., "CYGNSS: Enabling the future of hurricane prediction [remote sensing satellites]," *IEEE Geosci. Remote Sens. Mag.*, vol. 1, no. 2, pp. 52–67, Jun. 2013.

[63] A. R. Jacobson, X.-M. Shao, and R. H. Holzworth, "Satellite triangulation of thunderstorms, from fading radio fields synchronously recorded on two orthogonal antennas," *Radio Sci.*, vol. 46, no. 6, pp. 1–17, Dec. 2011.

[64] A. R. Jacobson and T. E. L. Light, "Bimodal radio frequency pulse distribution of intracloud-lightning signals recorded by the FORTE satellite," *J. Geophys. Res., Atmos.*, vol. 108, no. D9, May 2003, doi: 10.1029/2002JD002613.

[65] E. C. Bruning and D. R. MacGorman, "Theory and observations of controls on lightning flash size spectra," *J. Atmos. Sci.*, vol. 70, no. 12, pp. 4012–4029, Dec. 2013.

[66] N. Pailoor, "Evaluating the detection efficiency of VHF lightning emissions observed in low-Earth orbit," in *Proc. Amer. Geophyical Union Fall Meeting*, 2023. [Online]. Available: https://ntrs.nasa.gov/api/citations/20230017627/downloads/LANL_VHF_SNR_simulations_CubeSpark_Nihkil_AGU23.pdf

[67] L. E. Ott et al., "Production of lightning NO_x and its vertical distribution calculated from three-dimensional cloud-scale chemical transport model simulations," *J. Geophys. Res., Atmos.*, vol. 115, no. D4, Feb. 2010, doi: 10.1029/2009JD011880.

[68] W. J. Koshak, D. M. Mach, and P. M. Bitzer, "Mitigating VHF lightning source retrieval errors," *J. Atmos. Ocean. Technol.*, vol. 35, no. 5, pp. 1033–1052, May 2018.

[69] *The Global Observing System for Climate: Implementation Needs*, World Meteorological Organization, Geneva, Switzerland, 2016.

[70] M. Peterson, "Combined optical and radio-frequency perspectives on the time evolution of lightning measured by the FORTE satellite," *Earth Space Sci.*, vol. 9, Sep. 2022, Art. no. e2022EA00228.

Jackson R. Remington (Member, IEEE) received the B.S. degree in physics from Montana State University, Bozeman, MT, USA, in 2015, and the M.S. and Ph.D. degrees in physics from The University of Utah, Salt Lake City, UT, USA, in 2019 and 2021, respectively.

He was a NASA Post-Doctoral Fellowship under which he is currently working at the NASA Marshall Space Flight Center, Huntsville, AL, USA. His active research is in lightning physics, with a focus on developing detection algorithms for remote sensing platforms. His research interests include energetic radiation from thunderstorms and ultrahigh energy cosmic rays.

Patrick N. Gatlin (Member, IEEE) received the B.S. degree in meteorology from the University of South Alabama, Mobile, AL, USA, in 2002, and the M.S. and Ph.D. degrees in atmospheric science from The University of Alabama in Huntsville, Huntsville, AL, USA, in 2007 and 2014, respectively.

He is currently a Research Meteorologist with the NASA Marshall Space Flight Center (MSFC), Huntsville, where he conducts research in the areas of lightning and precipitation science and develops new thunderstorm remote sensing technology. He is a member of the NASA's Investigation of Cumulus Updrafts and ISS-Lightning Imaging Sensor Science Teams and works on NASA's Global Precipitation Measurement Mission. Prior to working at NASA, he was a Journeyman Weather Forecaster with NOAA's National Weather Service Forecast Office, Huntsville, AL, USA.

Sarah M. Stough received the B.S. degree in meteorology from The University of Oklahoma (OU), Norman, OK, USA, in 2012, and the M.S. and Ph.D. degrees in atmospheric science from The University of Alabama in Huntsville (UAH), Huntsville, AL, USA, in 2015 and 2020, respectively.

She worked as a Research Associate with the Earth System Science Center, UAH, from 2020 to 2024, on topics ranging from ground-based validation of satellite precipitation measurements to lightning measurement design concepts. She is currently a Research Scientist with the Cooperative Institute for Severe and High-Impact Weather Research and Operations (CIWRO), OU. Her research interests include operational applications of lightning data and kinematic, microphysical, and environmental relationships between lightning and deep convection.

Nikhil Pailoor received the B.S. degree in electrical engineering from the University of Washington, Seattle, WA, USA, in 2016, and the M.S. and Ph.D. degrees in electrical and computer engineering from Georgia Institute of Technology, Atlanta, GA, USA, in 2022.

He is currently a Post-Doctoral Researcher at Los Alamos National Laboratory, Los Alamos, NM, USA. His research interests have included radio remote sensing to detect lightning and lightning-induced phenomena in the ionosphere and the near-Earth space environment.

Sonja A. Behnke received the B.S. and Ph.D. degrees in physics (with dissertation in atmospheric physics) from New Mexico Institute of Mining and Technology, Socorro, NM, USA, in 2003 and 2013, respectively.

She is currently a Scientist at Los Alamos National Laboratory, Los Alamos, NM, USA, where she leads the development of a new radio frequency lightning sensor designed for CubeSats. Her research interests include radio frequency remote sensing of lightning, lightning mapping, and volcanic lightning.

Timothy J. Lang received the master's and Ph.D. degrees in atmospheric science from Colorado State University (CSU), Fort Collins, CO, USA, in 1997 and 2001, respectively.

He has worked as a Post-Doctoral Fellow at Harvard University, Cambridge, MA, USA, and a Research Scientist at CSU, before switching over to NASA in 2012. Currently, he is a Lead Research Aerospace Technologist with the NASA Marshall Space Flight Center, Huntsville, AL, USA, where he serves as the Mission Scientist for the International Space Station Lightning Imaging Sensor (ISS LIS). His research interests include thunderstorms, lightning, and microwave remote sensing.

Harald E. Edens received the M.Sc. degree in solid state physics from the University of Amsterdam, Amsterdam, The Netherlands, in 2002, and the Ph.D. degree in atmospheric physics from New Mexico Tech, Socorro, NM, USA, in 2011.

From 2011 to 2016, he worked at the Langmuir Laboratory, Socorro, as a Research Scientist, and an Assistant Professor with the Physics Department, New Mexico Tech, where he became the Director of the Langmuir Laboratory. He currently works with the ISR-2 Division, Los Alamos National Laboratory, Los Alamos, NM, USA. His research interests include lightning detection and mapping, remote sensing, atmospheric electric field measurements, optical detectors and imaging, instrumentation design, RF signal propagation, and electromagnetic compatibility.